Hindawi
Journal of Sensors
Volume 2021, Article ID 5596854, 9 pages
https://doi.org/10.1155/2021/5596854

Research Article

BPSK Modulation-Based Local Oscillator-Free IQ Demodulation for Millimeter Wave Imaging

Qibin Zheng,[1,2,3] **Yanpeng Jian**,[1,2] **Lei Wang**,[1] **Ziyue Ma**,[1] **Xinyu Li**,[4] **Chaofan Song**,[1,2] **Ping Li**,[2,3] **and Li Ding**[2,3]

[1]*Institute of Biomedical Engineering, University of Shanghai for Science and Technology, Shanghai 200093, China*
[2]*Terahertz Technology Innovation Research Institute, University of Shanghai for Science and Technology, Shanghai 200093, China*
[3]*Shanghai Institute of Intelligent Science and Technology, Tongji University, Shanghai 200092, China*
[4]*Shanghai Radio Equipment Research Institute, Shanghai 201109, China*

Correspondence should be addressed to Li Ding; sunnylding@usst.edu.cn

Received 18 January 2021; Revised 24 September 2021; Accepted 19 October 2021; Published 5 November 2021

Academic Editor: Antonio Lazaro

The precision of local oscillator (LO) signal in in-phase and quadrature (IQ) demodulation strongly affects the imaging performance of millimeter wave (mmWave) radars. Therefore, to eliminate the requirement for high-precision LO, a simple yet effective digital IQ demodulation method has been proposed with the aid of a specified sampling scheme in order to eliminate the demand for LO. Based on the bandpass sampling theorem, the characteristic of the intermediate frequency signal of mmWave imaging indicates that the LO is unrequired if the sampling rate is twice of the frequency of the carrier of the intermediate signal. In this way, the in-phase signal would be directly and accurately obtained by performing the Binary-Phase-Shift-Keying (BPSK) modulation on the samples, based on which the IQ demodulation would be completed by using the Hilbert transform. The proposed method does not employ LO and thus simplifies the demodulation process and is suitable for implementation in a Field-Programmable Gate Array (FPGA) with fewer hardware resources. To verify the method, a three-dimensional mmWave radar imaging is carried out at the 30-34 GHz bandwidth, where the sampling and digital IQ demodulation are realized by an ADC (AD9250) and FPGA (XC7K325T), respectively. The results show a simplified transceiver with lower requirements and the prospect of the proposed method being applied in radar imaging and other related fields.

1. Introduction

The millimeter wave (mmWave) technology, with its high resolution and the advantage of penetrability in dealing with insulating materials like paper, clothing, and fog, is now an important topic in radar imaging [1]. It has been applied in various fields, such as medical diagnostics [2, 3], security screening [4–6], military fields [7, 8], and nondestructive testing [9–12]. A vital component of these mmWave imaging systems is the in-phase and quadrature (IQ) demodulation which its performance can affect the imaging quality.

The conventional IQ demodulation in both analog and digital methods requires a local oscillator (LO) signal, whose accuracy and precision strongly affect the IQ demodulation performance [13]. However, the LO signal is inevitably deteriorated by some unfavourable drawbacks in the existing system. In the case of analog demodulation, both the inconsistency of analog devices and the variation of parameters with temperature fluctuation cause the phase imbalance of LO signal and highly limit the demodulation performance [14]. Moreover, the addition of individual analog devices (e.g., mixer and filter) further increases the power consumption and cost of the system. In the case of digital demodulation, the popular way to generate the LO signal is using the numerically controlled oscillator based on direct digital synthesis (DDS) [15, 16]. Currently, a look-up table-based DDS has the problems of relatively large signal spurious and low output frequency range. In order to solve the above problems, several methods have been proposed to achieve a high accuracy in real-time. For instance, [17] presents a direct

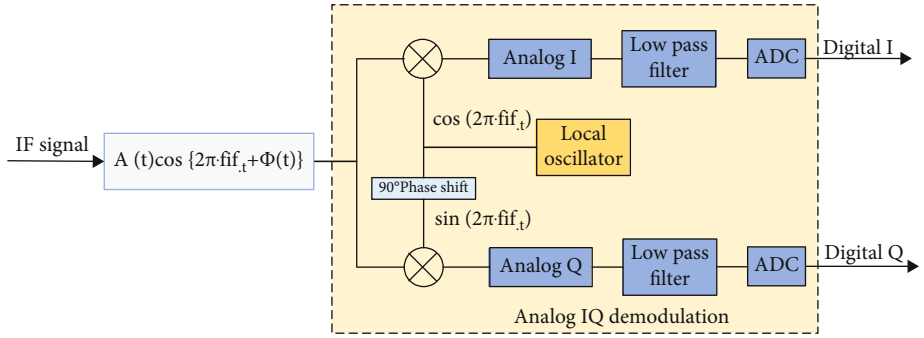

Figure 1: Traditional analog IQ demodulation with LO signals.

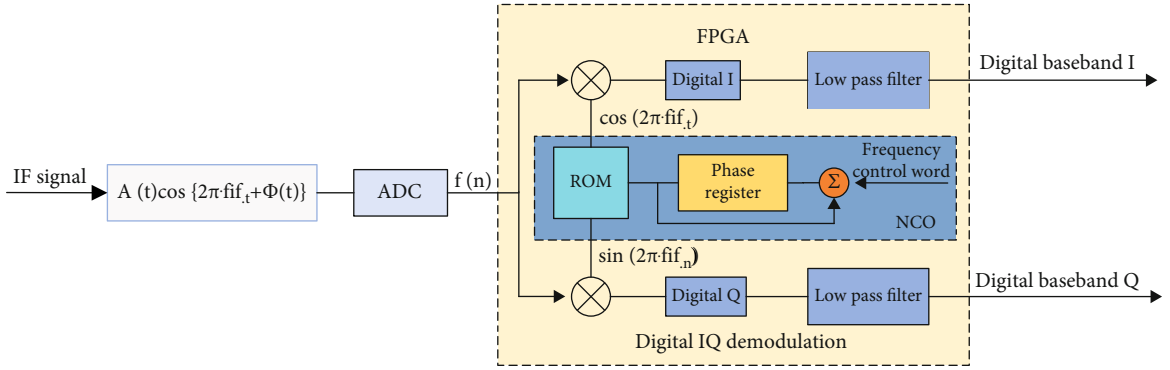

Figure 2: Traditional digital IQ demodulation with LO signals.

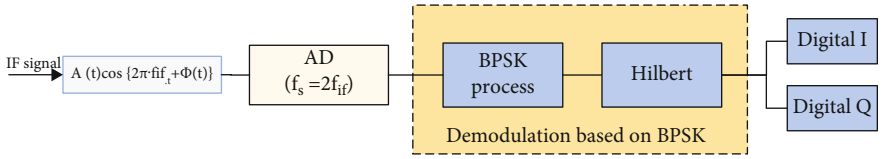

Figure 3: Block diagram of demodulation process based on the proposed BPSK modulation.

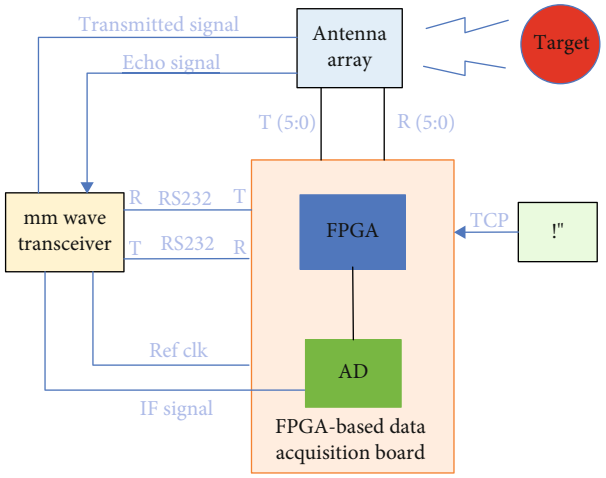

Figure 4: Block diagram of a 3D mmWave radar imaging system.

digital frequency synthesizer based on a Multipartite Table Method. The authors in [18] propose a novel direct digital frequency synthesis architecture based on the differential Coordinate Rotation Digital Computer algorithm. These methods improve the speed or accuracy of DDS to a certain degree. However, with the increasing precision requirement of LO, the DDS-based demodulation requires a large number of hardware resources and is hard to be implemented in FPGA [19]. Therefore, it is necessary to design a LO-free method for IQ demodulation, to reduce the hardware resources and simplify the design of the receiver.

In this paper, LO-free digital IQ demodulation for mmWave imaging has been proposed. Based on the band-pass sampling theorem, the analysis of mmWave echo reveals that setting the sampling rate at twice of the frequency of the carrier of the intermediate frequency (IF) echo, the sampled data reflect the characteristics of in-phase (I) signal. To this end, the proposed digital IQ demodulation has been implemented in two steps. Firstly, the I signal is obtained by directly performing Binary-Phase-Shift-

Figure 5: The setup of the 3D mmWave radar imaging system.

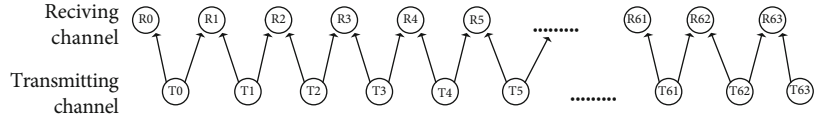

Figure 6: Scanning process diagram of antenna array x-direction antenna.

Table 1: Parameters of mmWave transceiver.

Parameter	Variable	Value
Staring frequency	f_0	30 GHz
Wavelength	λ	9.4 mm
RF bandwidth	B_{RF}	4 GHz
Pulse width	T	9 μs
IF bandwidth	B	100-130 MHz
IF carrier frequency	f_{if}	100 MHz

Keying (BPSK) modulation on the sampled data. Secondly, the Hilbert transform is applied on the obtained I signal to obtain the completed IQ demodulated data. The proposed IQ demodulation method eliminates the need for mixers against the traditional methods. Furthermore, this method has simplified digital demodulation and thus is easy to be implemented in FPGA. To verify the method, a three-dimensional (3D) mmWave radar imaging system operating at the 30-34 GHz bandwidth is set up. A 14-bit @ 200MSPS ADC chip (AD9250)-based data acquisition board is designed to sample the IF signal, where the IF carrier frequency is 100 MHz, and an FPGA (XC7K325T) is employed to control the system and achieve the proposed BPSK modulation-based LO-free IQ digital demodulation. The results demonstrate that the system realizes high-precision imaging and that the proposed method, with reduced hardware resources and simplified transceivers, has strong potential in the imaging field.

The structure of this paper is as follows: Section 2 explains the proposed demodulation method and the 3D mmWave radar imaging system. Section 3 presents the results of the experiment and performance analysis. Section 4 draws the conclusions of the paper.

2. Principles and System

2.1. BPSK Modulation-Based LO-Free IQ Digital Demodulation. The schematic diagrams of the traditional IQ demodulation in analog and digital are shown, respectively, in Figures 1 and 2. Both of these methods require an LO signal. In the analog demodulation method, the limitations of the device and the external environment make the LO signal hard to be synchronized with the ideal IF carrier signal and thus affect the demodulation accuracy [20]. While in the traditional digital demodulation, the digital LO signal is indispensable, generating a high-precision LO signal takes up a lot of FPGA resources [21]. In order to alleviate the pressure on FPGA hardware resources, the phase truncation method has been proposed to introduce additional noise and make the spurious suppression capability worse [21]. In

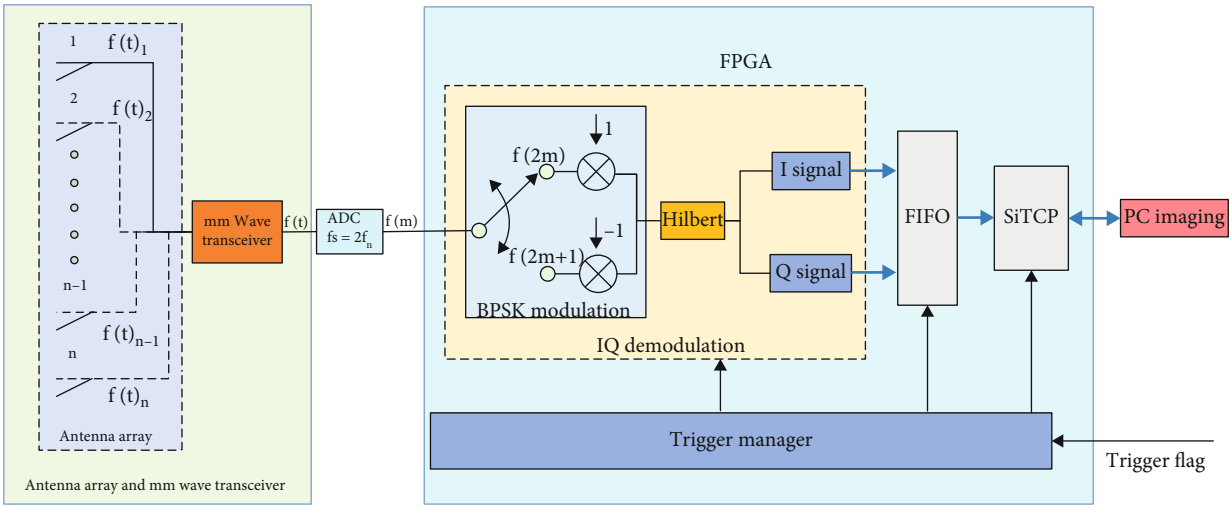

Figure 7: Block diagram of FPGA-based IQ demodulation without LO signals.

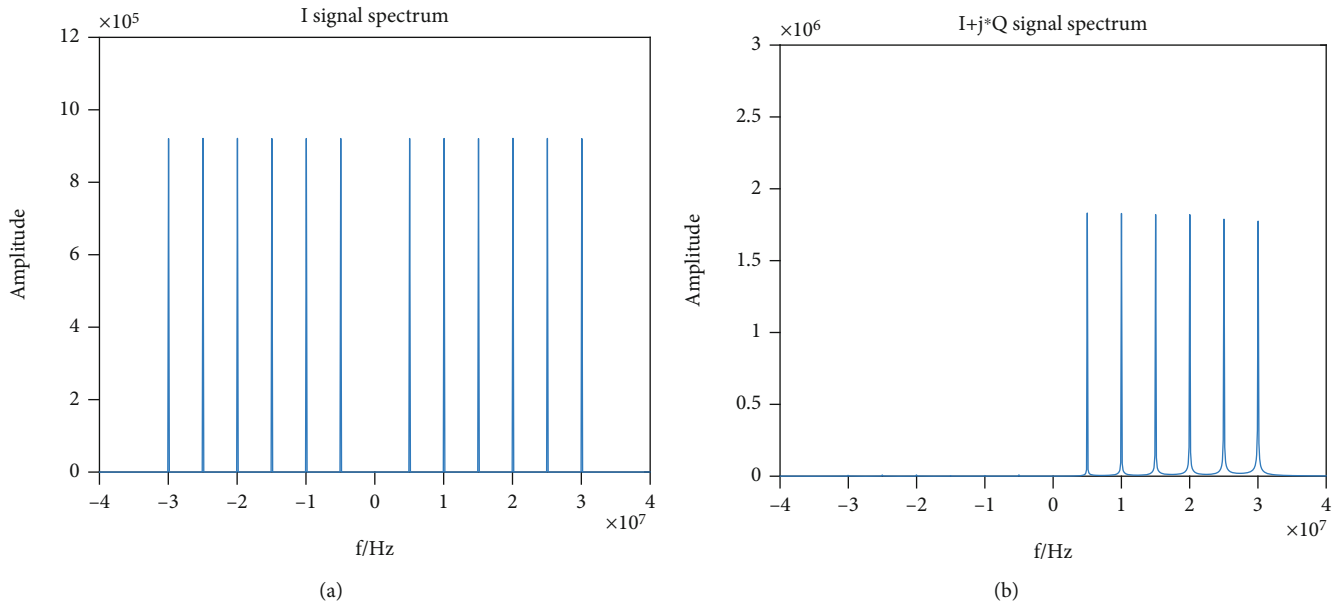

Figure 8: (a) Spectrum of performing the BPSK modulation on the sampled signal. (b) Spectrum of operating the Hilbert transform on the obtained I signal.

short, a high-performance LO signal increases the system complexity and cost but plays an important role in the traditional IQ demodulation methods.

Aiming at LO-free IQ demodulation and simplifying the receiver, the characteristic of the IF signal is analysed, and a new BPSK modulation-based IQ digital demodulation is proposed in this paper. As shown in Equation (1), the IF signal of mmWave radar imaging can be expressed in this form [22].

$$\begin{aligned} f(t) &= A\cos\{2\pi \cdot f_{\text{if}} \cdot t + \varphi(t)\} \\ &= A\cos(2\pi \cdot f_{\text{if}} \cdot t)\cdot\cos(\varphi(t)) - A\sin(2\pi \cdot f_{\text{if}} \cdot t)\cdot\sin(\varphi(t)), \end{aligned} \tag{1}$$

where f_{if} is the IF carrier's frequency, A is the scattering echo amplitude, and the $\varphi(t)$ is the target-echo phase information. According to bandpass sampling theorem, the sampling rate f_s must meet.

$$\begin{cases} \dfrac{2f_{\text{if}} + B}{n} \le f_s \le \dfrac{2f_{\text{if}}}{n-1}, \\ f_s \ge 2B. \end{cases} \tag{2}$$

If the sampling rate is twice the frequency of the carrier of the IF signal, i.e.,

$$f_s = 2f_{\text{if}}, \tag{3}$$

it can be observed that the IQ demodulation would be

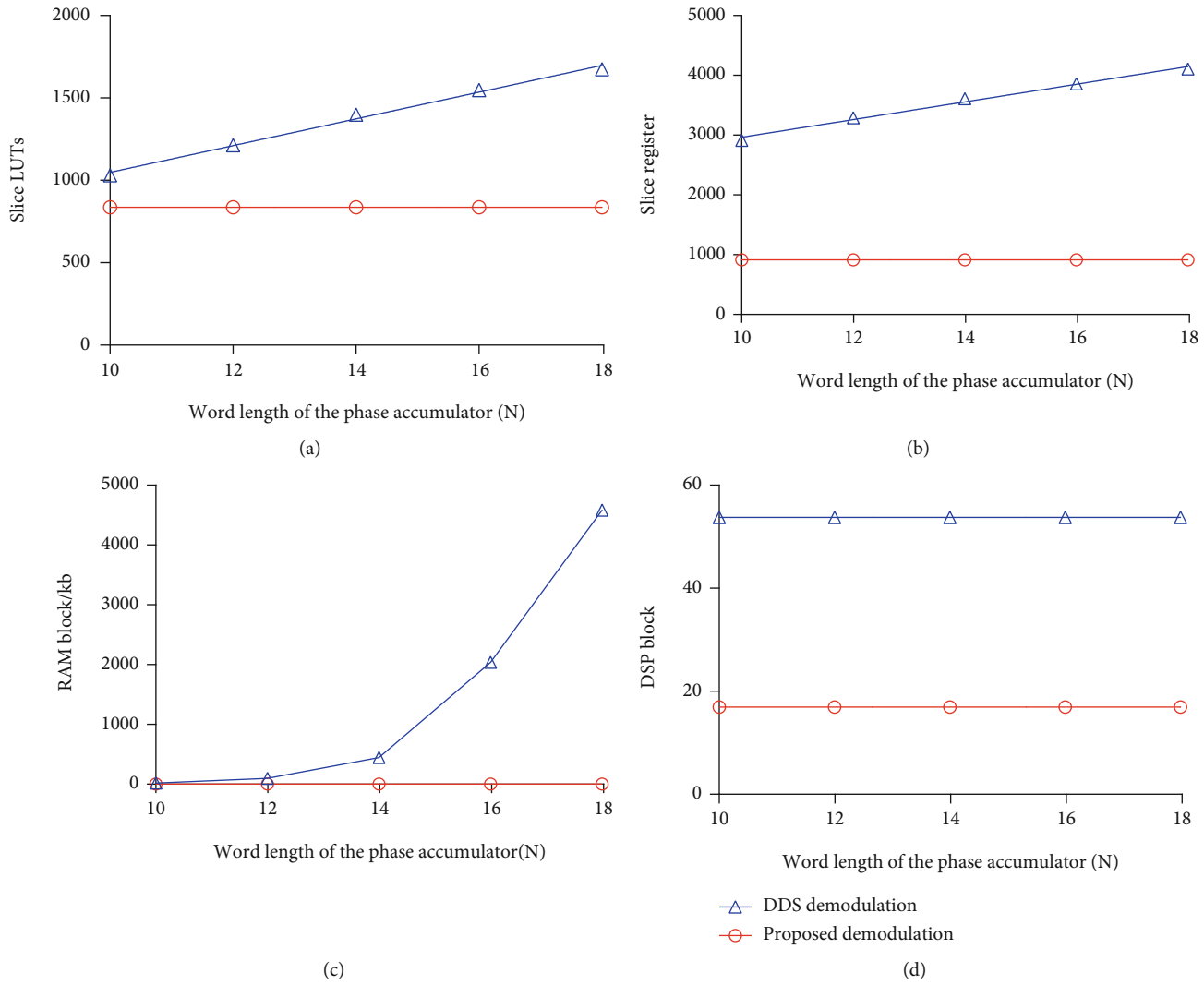

Figure 9: FPGA resource utilization for different word length of phase accumulator: (a) slice LUTs usage; (b) slice registers usage; (c) RAM block usage; (d) DSP block usage.

simplified by incorporating Equation (3) into Equation (1). Therefore, the IF signal can be expressed as:

$$\begin{aligned} f(m) &= A\cos\left(2\pi\cdot f_{\text{if}}\cdot\frac{1}{f_s}\cdot m\right)\cdot\cos\{\varphi(m)\} \\ &\quad - A\sin\left(2\pi\cdot f_{\text{if}}\cdot\frac{1}{f_s}\cdot m\right)\cdot\sin\{\varphi(m)\} \\ &= I(m)\cdot\cos(m\pi) - Q(m)\cdot\sin(m\pi), \end{aligned} \tag{4}$$

where $f(m)$ indicates the sampled data, $I(m) = A\cos\{\varphi(m)\}$ is the in-phase component, $Q(m) = A\sin\{\varphi(m)\}$ is the quadrature component, and $m = 0, 1, 2, \ldots$. Bringing the result of $\sin(m\pi) = 0$ into Equation (4), $I(m)$ can be represented as:

$$I(m) = \begin{cases} f(m) m \text{ is even}, \\ -f(m) m \text{ is odd}. \end{cases} \tag{5}$$

Equation (5) indicates that I signal demodulation could be easily obtained by performing the BPSK modulation on the sampled data, where BPSK keeps the phase of the even samples and reverses the sign of the odd samples. Then, the IQ demodulation would be completed by applying the Hilbert transform on the obtained I signal, $Q(m)$ signal is written as:

$$Q(m) = \text{Hilbert}\{I(m)\}. \tag{6}$$

From the above, the proposed BPSK modulation-based LO-free IQ digital demodulation is achieved. The detailed diagram of the method is given in Figure 3. The proposed method in this paper eliminates the requirement for high-precision LO and also greatly reduces the consumption of hardware resources.

2.2. Proof-of-Principle System. To verify the feasibility of this scheme, a 3D mmWave radar imaging system is set up. The block diagram and the imaging system are, respectively, shown in Figures 4 and 5. The system consists of a mmWave

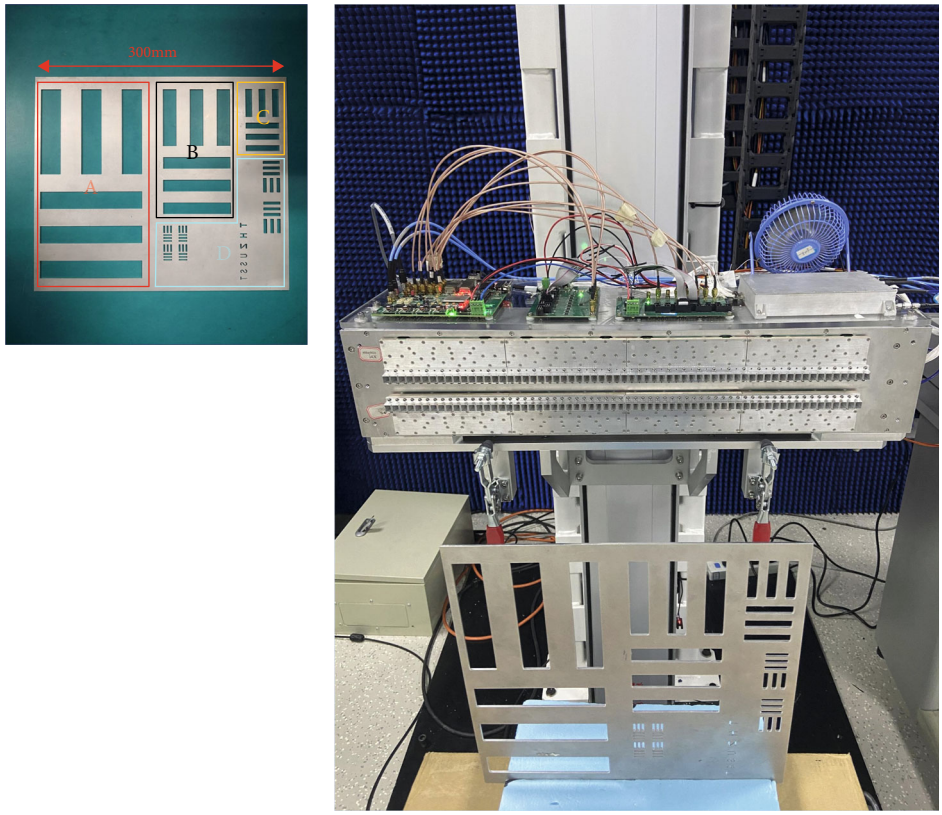

Figure 10: (a) Target area division. (b) Target test scene.

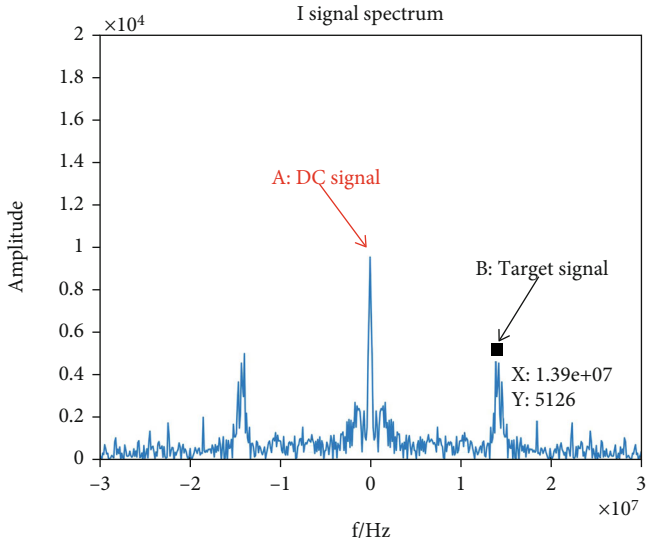

Figure 11: I signal spectrum of performing the BPSK modulation on the sampled signal.

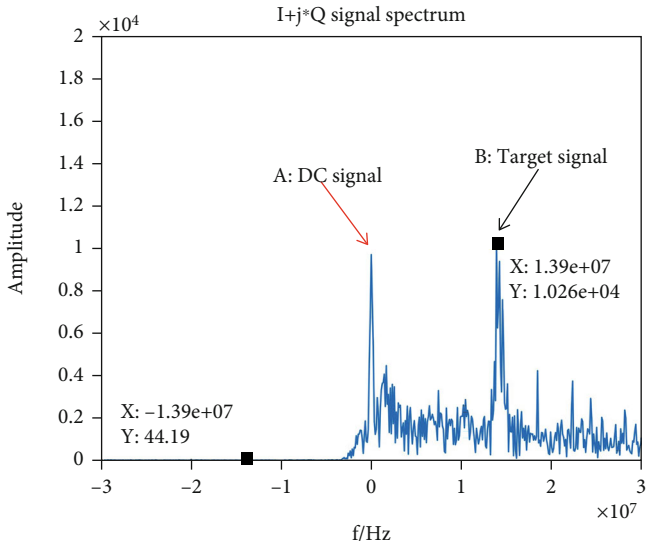

Figure 12: IQ complex signal spectrum of operating the Hilbert transform on the obtained I signal.

transceiver, an antenna array, and an FPGA-based data acquisition board. The mmWave transceiver transmits a sweep signal to the target through the array antenna, and the echo signal is downconverted to an IF signal, which contains information of the target. The entire system is controlled by the FPGA-based data acquisition board, which samples and processes the IF signal. At last, the processed data is transmitted to a personal computer (PC) for target imaging.

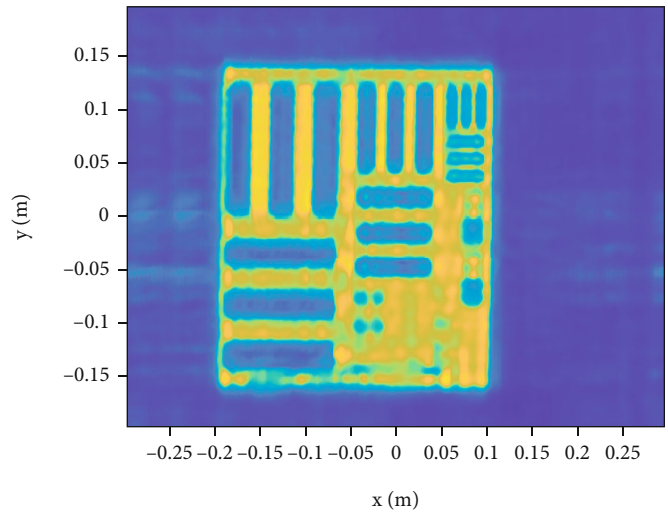

Figure 13: Imaging result of the mmWave radar imaging system.

2.2.1. Antenna Array and Signal Parameters. The antenna array includes 64 receive antennas and 64 transmit antennas in this 3D mmWave radar imaging system (as shown in Figure 5). Each transmit antenna radiates linear frequency modulation continuous wave signal. The synthesized aperture imaging is achieved by electrical scanning in horizontal direction and mechanical motion in vertical direction. As shown in Figure 6, this effective electrical scanning technique for synthesized aperture imaging has been incorporated into the system described in [23–26]. This system is configured to operate from 30 to 34 GHz, and the parameters of the mmWave transceiver in this system are shown in Table 1.

The electrical scanning in horizontal antenna array provides focusing only in horizontal direction, and a mechanical scan in the vertical direction is required for obtaining the focusing ability in the vertical direction. In this imaging system, the vertical mechanical scan step is half of the wavelength. Then, the popular range-migration algorithm is used to obtain high-resolution imaging [27].

2.2.2. FPGA-Based Data Acquisition Board. The FPGA-based data acquisition board has a reconfigurable logic in FPGA (XC7K325T), a ADC chip (AD9250), and several I/O interfaces, allowing users to flexibly control the system. The implementation of the proposed demodulation method is shown in Figure 7.

(1) Trigger manager module: control of the array antenna and the mmWave transceiver

(2) ADC sampling module: sample the IF signal

(3) IQ demodulation module: perform digital demodulation processing on the IF signal

(4) Ethernet module: transfer the IQ data to the PC through an Ethernet protocol realized in the FPGA

3. Experiments

3.1. Simulation Verification and Resource Consumption. The parameter setting is provided in Table 1, and six targets have been chosen with their IF locations at 105, 110, 115, 120, 125, and 130 MHz. The spectrum after BPSK processing and Hilbert transform are, respectively, shown in Figures 8(a) and 8(b). Through this figure, it can be seen that the proposed method can accurately move the IF signal to its baseband and achieve IQ demodulation without LO.

Figure 9 shows the FPGA resources consumed by the proposed method under different phase accumulator word lengths. With the increase of the word length of the phase accumulator, the slice LUTs and slice registers of DDS demodulation method increase linearly as shown Figures 9(a) and 9(b). Compared with DDS demodulation, the number of slice LUTs and slice registers in the proposed demodulation has been reduced by approximately 20 and 70%, respectively. As shown in Figure 9(c), the RAM increases exponentially in the DDS demodulation, but it is not consumed in the proposed demodulation. Compared with the DDS demodulation, the proposed demodulation only uses 70% of the DSP block, as seen from Figure 9(d). In the DDS demodulation, mixing will lead to the increase of data width, and the use of data truncation, for achieving fixed-point data processing, will cause spectrum spurious [28]. However, the proposed demodulation only needs symbol transformation and is not affected by the word length of phase accumulator. It does not produce the spectrum spurious caused by data bit fixed-point processing. At the same time, the required hardware resource is also reduced significantly.

3.2. Imaging Verification and Analysis. In this section, the proposed method was applied to the actual mmWave radar for 3D imaging, and an experimental target was imaged for verification. In the imaging experiment, the IQ demodulation part can run well under a 200 MHz system clock.

As shown in Figure 10(a), complex steel plate, divided into "A," "B," "C," and "D" parts and partially inserted into a foam, is used to test the imaging performance. The length/width of the A, B, and C areas is, respectively, 120/24, 80/16, and 40/8 mm. The width of area "D" is shorter than 4 mm which is beyond the system-resolution limitation as the mmWave transceiver has a frequency bandwidth of 30-34 GHz.

The target is located at 10 cm from the antenna plane in the experiment (as shown in Figure 10(b)). The IF frequency of the target can be calculated as 0.3 MHz; however, a frequency offset would be added, due to the nonignorable line-loss delay of the system. The frequency offset is tested as 13.6 MHz. Therefore, the output frequency of the IF signal would be 100 + 13.6 + 0.3 = 113.9 MHz.

The I signal spectrum obtained after sampling and BPSK processing of the signal is shown in Figure 11, in which the "A" signal is a direct-current (DC) signal, and the "B" signal is a target signal. It can be seen from Figure 11 that after BPSK modulation, the IF carrier signal with a frequency of 100 MHz can be removed accurately to complete I channel demodulation. Therefore, the target signal frequency is 13.9 MHz. Then, the Hilbert transform is used to obtain the IQ signal and IQ complex signal spectrum as shown in Figure 12. The image rejection ratio [29] of BPSK-based IQ demodulation reaches 55 dB, which can meet the requirements of the actual millimeter wave radar imaging system [30].

Figure 13 is the imaging result, which indicates that parts "A," "B," and "C" are imaged clearly (the image of "D" area was blurred due to its size beyond the system-resolution limitation). The results are consistent with the theoretical situation, where the theoretical resolutions of azimuth dimension, height dimension, and range dimension are, respectively, 4.9, 5.2, and 3.75 mm. Furthermore, the bottom part of the target inserted into the foam can be imaged well and shows the good penetrability of mmWave.

4. Conclusions

Future mmWave imaging radar receivers require faster processing speed and higher accuracy. However, the existing digital IQ demodulation methods rely on the LO signal which is typically generated using the DDS, resulting in problems of relatively large signal spurious and low output frequency range, thereby restricting the radar speed or accuracy. This paper has presented a simple yet effective method to achieve a digital IQ demodulation in mmWave radar system which eliminates the LO signal and simplified the design of radar transceivers. Using a 3D mmWave radar imaging system, the proposed method has been validated with a good performance. The findings indicate that the proposed method has strong application potentials in the radar and imaging fields.

Data Availability

The test data, simulation data, and the proposed method used to support the findings of this study are available from the corresponding author upon request. The algorithm proposed in this paper does not involve any patent problems.

Conflicts of Interest

The authors declare no conflict of interest.

Acknowledgments

This work was supported in part by the National Key R&D Program of China (2018YFF01013003), in part by the National Natural Science Foundation of China (61731020 and 12105177), in part by the 111 Project (D18014), in part by the International Joint Lab Program supported by Science and Technology Commission of Shanghai Municipality (17590750300), and in part by the Key Project Supported by Science and Technology Commission of Shanghai Municipality (YDZX20193100004960).

References

[1] M. C. Kemp, "Detecting hidden objects: security imaging using millimetre-waves and terahertz," in *2007 IEEE Conference on Advanced Video and Signal Based Surveillance*, pp. 7–9, London, UK, 2007.

[2] L. Chao and M. N. Afsar, "Millimeter wave dielectric spectroscopy and breast cancer imaging," in *2012 Conference on Precision electromagnetic Measurements*, pp. 572–575, Amsterdam, Netherlands, 2012.

[3] S. D. Meo, G. Matrone, and M. Pasian, "High-resolution mm-Wave imaging techniques and systems for breast cancer detection," in *IEEE MTT-S International Microwave Workshop Series on Advanced Materials and Processes for RF and THz Applications*, pp. 1–3, Pavia, Italy, 2017.

[4] X. Zhuge and A. G. Yarovoy, "A sparse aperture MIMO-SAR-based UWB imaging system for concealed weapon detection," *IEEE Transactions on Geoscience and Remote Sensing*, vol. 49, no. 1, pp. 509–518, 2011.

[5] S. Ahmed, A. Schiessl, F. Gumbmann, M. Tiebout, S. Methfessel, and L.-P. Schmidt, "Advanced microwave imaging," *Microwave Magazine IEEE*, vol. 13, no. 6, pp. 26–43, 2012.

[6] M. E. Yanik and M. Torlak, "Near-field 2-D SAR imaging by millimeter-wave radar for concealed item detection," in *IEEE Radio and Wireless Symposium*, pp. 1–4, Orlando, FL, USA, 2019.

[7] V. I. Antyufeev, V. N. Bykov, and A. M. Grichaniuk, "Radiometric observability estimation of military equipment samples in a millimeter-wave band," in *International Kharkov Symposium on Physics & Engineering of Microwaves IEEE*, vol. 1, pp. 196–198, Kharkov, Ukraine, 2004.

[8] U. S. Jha, "The millimeter Wave (mmW) radar characterization, testing, verification challenges and opportunities," in *IEEE AUTOTESTCON*, pp. 1–5, National Harbor, MD, USA, 2018.

[9] R. Zoughi, S. Kharkovsky, and F. Hepburn, "Microwave and millimeter wave testing for the inspection of the space shuttle spray on foam insulation (SOFI) and the acreage heat tiles," *International Human Resources Development Corp*, vol. 280, no. 1, pp. 439–446, 2006.

[10] S. Shrestha, S. Kharkovsky, and R. Zoughi, "Microwave and millimeter wave nondestructive testing of the space shuttle external tank insulating foam," *Materials Evaluation*, vol. 63, no. 3, pp. 339–344, 2005.

[11] S. Kharkovsky, J. T. Case, and R. Zoughi, "Millimeter wave detection of localized anomalies in the space shuttle external fuel tank insulating foam and acreage heat tiles," in *IEEE Instrumentationand Measurement Technology Conference Proceedings*, pp. 1527–1530, Ottawa, Ont, Canada, 2005.

[12] M. Kim, J. Kim, H. Kim et al., "Nondestructive high spatial resolution imaging with a 60 GHz near-field scanning millimeter-wave microscope," *Review of Scientific Instruments*, vol. 75, no. 3, pp. 684–688, 2004.

[13] E. D. Adler, E. A. Viveiros, and M. C. Bartlett, "Direct digital synthesis applications for radar development," in *Proceedings International Radar Conference*, pp. 224–226, Alexandria, VA, USA, 1995.

[14] D. Qian, Z. Ping, and Q. Haiming, "Bandpass sampling and quadrature demodulation in synthetic aperture radar," in *CIE International Conference on Radar*, pp. 1–4, Shanghai, China, 2006.

[15] Z. Zhu, H. Quan, and L. Tian, "The design of NCO built in ultra-high-speed data converter," in *IEEE 3rd International Conference on Electronics Technology*, pp. 319–323, Chengdu, China, 2020.

[16] R. Ertl and J. Baier, "Increasing the frequency resolution of NCO-systems using a circuit based on a digital adder," *in IEEE Transactions on Circuits and Systems II: Analog and Digital Signal Processing*, vol. 43, no. 3, pp. 266–269, 1996.

[17] A. G. M. Strollo, D. D. Caro, and N. Petra, "A 630 MHz, 76 mW direct digital frequency synthesizer using enhanced ROM compression technique," *IEEE Journal of Solid-State Circuits*, vol. 42, no. 2, pp. 350–360, 2007.

[18] C. Y. Kang and E. E. Swartzlander, "Digit-pipelined direct digital frequency synthesis based on differential CORDIC," *IEEE Transactions on Circuits & Systems I Regular Papers*, vol. 53, no. 5, pp. 1035–1044, 2006.

[19] G. P. Ao, "The basic principle and FPGA implementation of NCO," in *Second International Conference on Instrumentation, Measurement, Computer, Communication and Control*, pp. 90–94, Harbin, 2012.

[20] J. Meng, H. Wang, P. Ye et al., "I/Q linear phase imbalance estimation technique of the wideband zero-IF receiver," *Electronics*, vol. 9, no. 11, p. 1787, 2020.

[21] Z. Li, T. Chu, Y. Wang et al., "Complete analysis of the spurious spectrum of DDS in the presence of phase truncation," in *IEEE/INFORMS International Conference on Service Operations, Logistics and Informatics*, pp. 439–442, Chicago, IL, USA, 2009.

[22] F. Bandiera, A. Coluccia, V. Dodde, A. Masciullo, and G. Ricci, "CRLB for I/Q imbalance estimation in FMCW radar receivers," *IEEE Signal Processing Letters*, vol. 23, no. 12, pp. 1707–1711, 2016.

[23] D. M. Sheen, D. L. McMakin, and T. E. Hall, "Three-dimensional millimeter-wave imaging for concealed weapon detection," *in IEEE Transactions on Microwave Theory and Techniques*, vol. 49, no. 9, pp. 1581–1592, 2001.

[24] D. M. Sheen, D. L. McMakin, and T. E. Hall, "Near field imaging at microwave and millimeter wave frequencies," in *IEEE/MTT-S International Microwave Symposium*, pp. 1693–1696, Honolulu, HI, 2007.

[25] D. M. Sheen, D. L. McMakin, and T. E. Hall, "Near-field three-dimensional radar imaging techniques and applications," *Applied Optics*, vol. 49, no. 19, pp. 83–93, 2010.

[26] Y. Fujii, Y. Fujiwara, and Y. Yanase, "Nondestructive detection of termites using a millimeter-wave imaging technique," *Forest Products Journal*, vol. 57, no. 10, pp. 75–79, 2007.

[27] Z. Wang, Q. Guo, X. Tian, T. Chang, and H.-L. Cui, "Near-field 3-D millimeter-wave imaging using MIMO RMA with range compensation," *in IEEE Transactions on Microwave Theory and Techniques*, vol. 67, no. 3, pp. 1157–1166, 2019.

[28] V. F. Kroupa, V. Cizek, J. Stursa, and H. Svandova, "Spurious signals in direct digital frequency synthesizers due to the phase truncation," *IEEE Transactions on Ultrasonics Ferroelectrics and Frequency Control*, vol. 47, no. 5, pp. 1166–1172, 2000.

[29] S. Lerstaveesin and B. S. Song, "A complex image rejection circuit with sign detection only," *IEEE Journal of Solid-State Circuits*, vol. 41, no. 12, pp. 2693–2702, 2006.

[30] L. Der and B. Razavi, "A 2-GHz CMOS image-reject receiver with LMS calibration," *IEEE Journal of Solid-State Circuits*, vol. 38, no. 2, pp. 167–175, 2003.